

RESEARCH ARTICLE

Dissolvable microneedle patch enables local delivery of immunomodulatory microparticles containing bifunctional molecules for periodontal tissue regeneration

Xuexiang Zhang¹ · Mohammad Mahdi Hasani-Sadrabadi¹ · Erfan Dashtimighadam² · Farahnaz Fahimipour³ · Bhumika Shokeen⁴ · Olga Bezouglaia⁵ · Ruxing Fu^{1,6} · Isabelle Hong¹ · Yang Yang^{6,7} · Tara Aghaloo⁵ · Benjamin M. Wu^{1,6,7,8,9} · Zhen Gu^{1,7,10} · Renate Lux⁴ · Song Li¹ 

Received: 24 January 2024 / Revised: 30 April 2024 / Accepted: 20 May 2024
© The Author(s) 2024

Abstract

Periodontitis is initiated by dysbiosis of the oral microbiome. Pathogenic bacteria elicit ineffective immune responses, which damage surrounding tissues and lead to chronic inflammation. Although current treatments typically aim for microbial eradication, they fail to address the significance of immune cell reactions in disease progression. Here, we searched for small molecules as drug candidates and identified a bifunctional antibiotic, azithromycin (AZM), that not only inhibits bacterial growth but also modulates immune cells to suppress inflammation. We further engineered a dissolvable microneedle patch loaded with biodegradable microparticles for local and painless delivery of AZM to the gingival tissues. Inflammatory cytokines were decreased while anti-inflammatory cytokines and M2 macrophage were increased with AZM treatments in vitro. In vivo delivery of the AZM-loaded microneedle patch demonstrated the same effects on cytokine secretion and the promotion of tissue healing and bone regeneration. In addition, microparticles containing anti-inflammatory interleukin-4 alone or in combination with separately-formulated AZM microparticles, had similar or slightly enhanced therapeutic outcomes respectively. The bimodal action of AZM obviates the necessity for separate antibacterial and immunomodulatory agents, providing a practical and streamlined approach for clinical treatment. Our findings also demonstrate the therapeutic

✉ Song Li
songli@ucla.edu

¹ Department of Bioengineering, University of California, Los Angeles (UCLA), CA 90095, USA

² Symphony Biosciences, Birmingham, AL 35294, USA

³ Department of Periodontology, School of Dentistry, University of Alabama, Birmingham, AL 35233, USA

⁴ Section of Biosystems and Function, UCLA School of Dentistry, Los Angeles, CA 90095, USA

⁵ Division of Diagnostic and Surgical Sciences, UCLA School of Dentistry, Los Angeles, CA 90095, USA

⁶ Department of Materials Science and Engineering, University of California, Los Angeles, CA 90095, USA

⁷ California Nano Systems Institute, University of California, Los Angeles, CA 90095, USA

⁸ Section of Advanced Prosthodontics, School of Dentistry, University of California, Los Angeles, CA 90095, USA

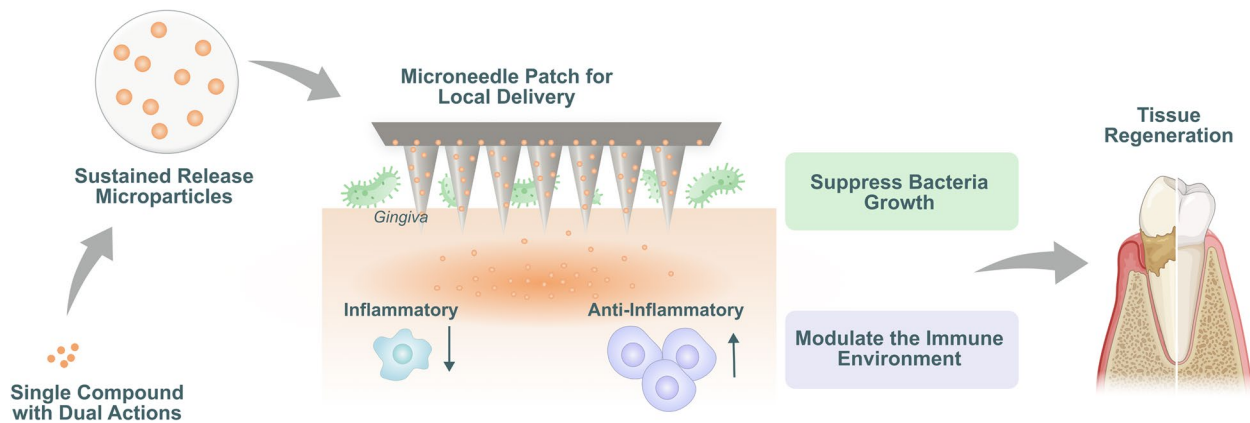
⁹ The ADA Forsyth Institute, Cambridge, MA 02142, USA

¹⁰ Key Laboratory of Advanced Drug Delivery Systems of Zhejiang Province, College of Pharmaceutical Sciences, Zhejiang University, Hangzhou 310058, China



efficacy of microparticles delivery into the soft tissues by a minimally invasive and fast-degrading microneedle patch and offer a novel therapeutic approach for the treatment of periodontitis and other diseases through immunomodulation.

Graphical Abstract



Highlights

- Dual actions of a single compound with both antibiotic and immunomodulatory effects can suppress inflammation and promote tissue regeneration.
- Fast-dissolving microneedle patch enables minimally invasive and local delivery of biodegradable microparticles as distributive depots for sustained release of therapeutics in diseased tissues.

Keywords Microneedle · Immunomodulation · Local drug delivery · Chronic inflammation · Tissue regeneration

Introduction

Periodontal disease, also known as gum disease, is a microbiome-induced chronic inflammatory condition that affects the supporting structures of teeth, including the gingiva, periodontal ligament, cementum and bone [1]. It is so common that it affects about 50% of the adults over the age of thirty globally [2]. In healthy individuals, the oral microbiome is in a state of homeostasis with the host. However, when the overall microbiome balance is disrupted, the resulting polymicrobial synergy and dysbiosis can trigger inflammatory and inadequately regulated immune responses which eventually evolve into chronic inflammation and ultimately tissue destruction and bone loss [1, 3, 4]. Thus, although bacteria are the initiator, the host immune system plays a vital role in disease progression. In recent years, immunomodulation has started to gain attention for treating periodontitis [5].

Pathogenic bacteria have developed numerous different strategies to counteract the normal immune responses and exacerbate the disease through virulence factors and pro-inflammatory mediators [3, 6]. For instance, *Porphyromonas gingivalis* utilizes lipopolysaccharide, proteases, fimbriae, and other virulence factors, to enhance bacterial colonization and support the growth of the surrounding microbial

biofilm community. Gingipains, a class of proteases, can degrade host proteins including collagen a main structural matrix protein necessary for tissue regeneration and complement components which comprise an important part of innate immune response [7]. Gingipains also elicit pro-inflammatory signaling pathways to promote chronic inflammation thus preventing tissue healing and regeneration [8]. Gingipains along with other virulence factors play a crucial role in promoting coaggregation of *P. gingivalis* with other bacteria and facilitating the formation of dental biofilm [6]. Through evolution, pathogenic bacteria have developed the ability to evade host immune responses and skew appropriate immune reaction. Moreover, the accumulation of bacteria allows biofilm formation, which creates a protected environment for the bacteria by hindering immune clearance and exacerbating the inflammatory response.

Another important factor for periodontitis progression is the behavior of immune cells, such as neutrophils, macrophages, and T cells [9–13]. They respond to the presence of bacterial pathogens by releasing cytokines and chemokines that trigger inflammatory responses. In the early stage of periodontitis, neutrophils are the first line of defense against bacteria. They clear the pathogens by phagocytosis and can become apoptotic after engulfing microbes, form a

“wall” between the junctional epithelium and the pathogen-rich dental plaque and use neutrophil extracellular traps (NETs) to capture bacteria [11]. Macrophages including tissue-resident and monocyte-derived macrophages also play a defending role against bacterial infection. They can clear apoptotic neutrophils, phagocytose microbes, release pro-inflammatory cytokines and present antigens to stimulate T cells [9]. In response to different sets of inducing factors, macrophages are polarized to various functional phenotypes – M1 and M2 are two representative phenotypes of inflammatory and anti-inflammatory macrophages respectively. M1 macrophages secrete high level of inflammatory mediators such as tumor necrosis factor- α (TNF- α) and interleukin (IL)-6 contribute significantly to tissue damage and bone resorption, while M2 macrophages are associated with anti-inflammatory cytokines such as IL-10, arginase-1, and transforming growth factor (TGF) that promote tissue remodeling and regulate the resolution of inflammation [14].

T cells have many subsets with different functions. The T helper 17 (T_H17) cell subset has been shown to be a major player in pathogenesis of periodontitis [15]. Persistent T_H17 activation produces high level of pro-inflammatory cytokines, promotes the differentiation of osteoclasts and induces the production of matrix metalloproteinases (MMPs) [12, 13]. Osteoclast activity leads to bone resorption and MMPs degrade the extracellular matrix needed for tissue regeneration. On the other hand, T regulatory (T_{Reg}) cells are immune regulators that help prevent excessive inflammation by suppressing the activity of other immune cells. However, their functions are impaired, and their numbers are reduced in chronic periodontitis [16].

Neutrophils, M1 macrophages and T_H17 cells further play a role together in alveolar bone destruction *via* NLRP3 inflammasome. Inappropriate inflammasome activation increases osteoclast activity, decreases osteoblast activity, and promotes inflammation [17]. Chronic inflammation disrupts the osteoblasts/osteoclasts balance and results in bone loss [14, 18].

Recognizing the significance of addressing both bacterial and immune-related aspects in the treatment of periodontitis, we aimed to develop a comprehensive approach. Recently we demonstrated the therapeutic effects of treating periodontitis with both antibiotics and immune modulatory cytokines [19]. However, cost, safety concerns and regulatory complications for enclosing a protein immune modulatory drug (i.e., IL-4) are barriers for clinical use of this approach. Therefore, we searched for small molecule candidate drugs, which are stable during material formulation and sustained release, have anti-bacterial properties, and can induce the transition of macrophage phenotype from M1 to M2 to promote tissue regeneration. Here we identified the antibiotic azithromycin (AZM) as having the desired dual

effect on both bacteria and immune cells [20–22]. AZM has been shown to polarize macrophages to an M2 phenotype *via* inhibition of the STAT1, NF- κ B and PI3K/Akt signaling pathways [21, 22]. To facilitate targeted delivery, we encapsulated AZM in microparticles (MP) and incorporated these AZM MPs into dissolvable microneedle (MN) patches [23, 24]. Leveraging the MN patches as a delivery platform allowed for efficient tissue penetration, more uniform distribution, and localized retention of MPs at the affected gingival sites. This patch-based application offers convenience to patients, enhancing compliance and enabling early intervention. Simply put, the MN patch is applied to the diseased gum, where micron-scale needles penetrate the tissue, allowing the patch matrices to dissolve and leaving the embedded MPs within the tissue for sustained release of therapeutic agents.

Results

Screening of bi-functional small molecules

Based on our selection criteria for small molecular immunomodulatory drugs that have documented ability to polarize macrophages towards the M2 phenotype, we tested the following four most promising candidate drugs—*azithromycin*, *tofacinib*, *lupeol* and *dexamethasone*. All of them have been reported to repolarize the macrophage towards M2 phenotype in various disease models [20–22, 25–27]. On top of being anti-inflammatory immune modulators, azithromycin (AZM) is an antibiotic [28]; tofacitinib is a Janus Kinase (JAK) inhibitor that can suppress the expression of IL-6 [29]; lupeol is an anti-inflammatory natural product [30]; and dexamethasone is a widely used glucocorticoid [31].

In bone marrow-derived macrophages (BMDMs), all four of the selected immunomodulators significantly suppressed the overall immune reaction by reducing the expression of the inflammatory marker inducible nitric oxide synthase (iNOS) (Fig. 1a). Cytotoxicity on primary macrophages was observed at 333 μ M for AZM, at 200 μ M for tofacitinib, at 100 μ M for lupeol and at all concentrations for dexamethasone (Fig. S1). A recent study also showed dexamethasone induced ROS generation and mitochondria-dependent apoptosis in RAW 264.7 cells *via* the Krüppel-like factor 9 (KLF9) [32]. While tofacitinib, lupeol and dexamethasone did not show any antibacterial effects against *Aggregatibacter actinomycetemcomitans* (*A.a.*) as tested in agar plates (Fig. 1b), the efficacy of AZM against the periodontal bacteria *A.a.* and *P. gingivalis* was confirmed with the Kirby diffusion assay, and the efficacy is comparable with the clinically used antibiotic minocycline (Fig. S2). Comparing AZM with the conventional tetracycline (TTC) class of antibiotics [33],

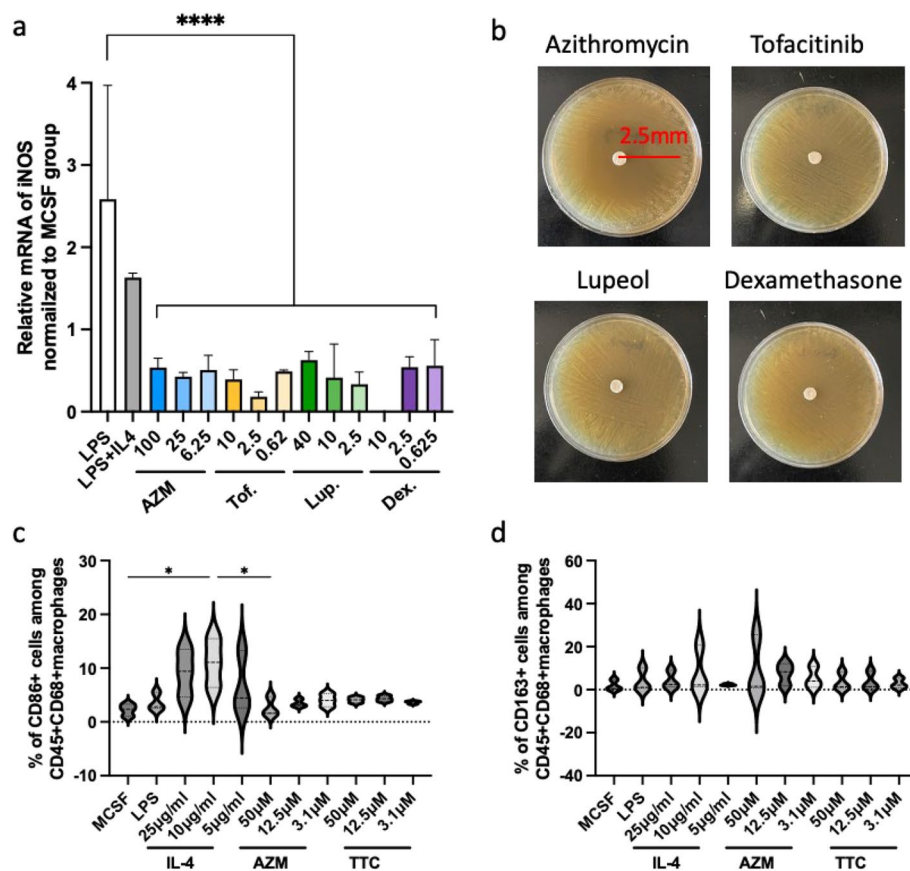


Fig. 1 Screening of small molecules for macrophage polarization. **a** Screening of four selected immunomodulatory small molecules (“AZM” = azithromycin, “Tof.” = tofacitinib, “Lup.” = lupeol and “Dex.” = dexamethasone) by qPCR of iNOS expression on mouse bone marrow-derived macrophages (BMDMs). All data are presented as mean \pm SD ($n = 3$). **b** Antibacterial properties of the compounds on the oral bacterium *A.a.* was measured by inhibition zone on agar plates. The red line indicates the radius of the inhibition zone. **c** and **d** Present the percentage of CD86⁺ M1 macrophages and CD163⁺ M2 macrophages measured by flow cytometry on primary rat BMDMs. For the MCSF group, macrophages were grown in macrophage colony-stimulating factor (MCSF); the LPS group was stimulated with lipopolysaccharide (LPS) for 6 h; and two antibiotics—AZM (azithromycin) and TTC (tetracycline) treatments were analyzed after stimulation with LPS for 6 h. $n = 3$

AZM altered macrophage polarization towards an anti-inflammatory CD163⁺ M2 phenotype, whereas TTC did not trigger a similar immune modulatory response (Fig. 1c, d). The gating strategy for flow cytometry is shown in Fig. S3.

Design and characterization of the AZM-MN patch

To achieve sustained release of AZM for a prolonged effect, we loaded AZM into biodegradable poly(lactic-co-glycolic acid) (PLGA) MPs. We then embedded AZM MPs into the dissolvable MN patch made of polyvinylpyrrolidone (PVP) to achieve painless and suture-free delivery of MPs into the gingival tissue (Fig. 2a). PVP is a biocompatible and water-soluble polymer, which allows sharp needle formation and has been used in various drug delivery applications [34–37]. As shown in the schematic in Fig. 2b, the AZM-MN patches can be applied to the diseased gum. The needles and the base

dissolves within 10 min [19], leaving the embedded particles in the tissue.

We used a single emulsion fabrication method to generate AZM MPs with an average size of 5 μ m (Fig. 2c, d). For comparison, we also used a double emulsion method to preserve protein activity and generate IL-4 PLGA MPs (as positive control) with a similar size to the AZM-MP. Moreover, various inherent viscosities of PLGA 50:50 were examined, and 0.6 dl/g PLGA was selected since a release time of around a week was desired (Fig. S4). Release of AZM and IL-4 from MPs also evaluated *in vitro* (Fig. 2e).

MPs were then mixed with PVP, cast on the molds, and dried at room temperature overnight. Dried MN patches were peeled off from the mold. The resulting MNs were pyramid shaped with 200 μ m \times 200 μ m (base) \times 750 μ m (height) in dimension, as shown in the electron microscopy images (Fig. 2f). The MPs were distributed evenly in needles, while in

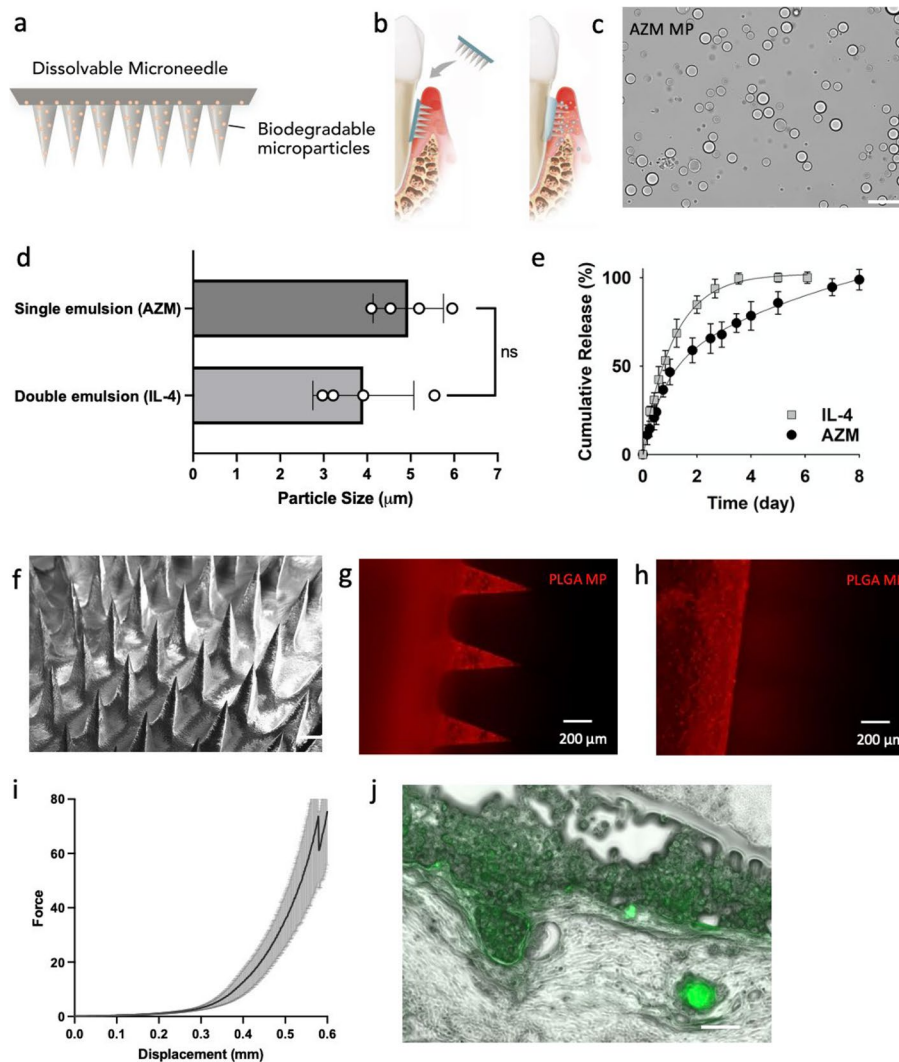


Fig. 2 Physical Characterization of PVP microneedle. **a** Schematic depicting the design of dissolvable PVP MN loaded with biodegradable PLGA MPs. **b** Schematics of MN administration, dissolution and drug release. **c** Representative bright field image of AZM MPs. Scale bar of 50 μm . **d** Size distribution of AZM and IL-4 MPs made using single emulsion and double emulsion methods, respectively. All data are presented as mean \pm SD ($n=4$). **e** Cumulative in vitro release of AZM and IL-4 from MPs at 37 $^{\circ}\text{C}$ and pH 7.4. **f** SEM image of microneedles loaded with MPs. Scale bar of 200 μm . **g**, **h** Distribution of fluorescent MPs in needle tips and the base, respectively. Scale bar represents 200 μm . **i** Mechanical strength of the microneedles measured by Instron machine. All data are presented as mean \pm SD ($n=4$). **j** Penetration of microneedle loaded with FITC-dextran PLGA MP into fresh rat gingival tissues. Scale bar of 200 μm

the base more particles were present closer to the needle due to gravity during fabrication process (Fig. 2g, h). The mechanical properties of MNs are critical for tissue penetration. A compression test of MNs indicated sufficient mechanical strength to penetrate freshly extracted rat gingival tissues (Fig. 2i, j).

In vitro evaluation of MN patches

Effective bacterial killing of the periodontal pathogen *P. gingivalis* was observed in liquid culture using supernatants from PBS-immersed AZM-MNs for up to 30 days (Fig. 3a, b). Biofilm-forming oral bacteria such as *A.a.* can facilitate

accumulation of pathogenic microbiomes and form difficult to eradicate biofilms on surfaces [38]. The inhibition zone formed by placing AZM-MN patches on agar plates were examined to test the efficacy of antibiotics released from the patch. Clear inhibition zones were observed around the square MN patches in both *P. gingivalis* and *A.a.* culture plates, and representative images are shown in Fig. 3c, d (full set of data in Fig. S5).

Furthermore, we investigated the immunomodulatory effects of AZM in its soluble form, as particles, and when loaded into MN patches using human peripheral blood mononuclear cells (PBMCs), which consist of a mixture of

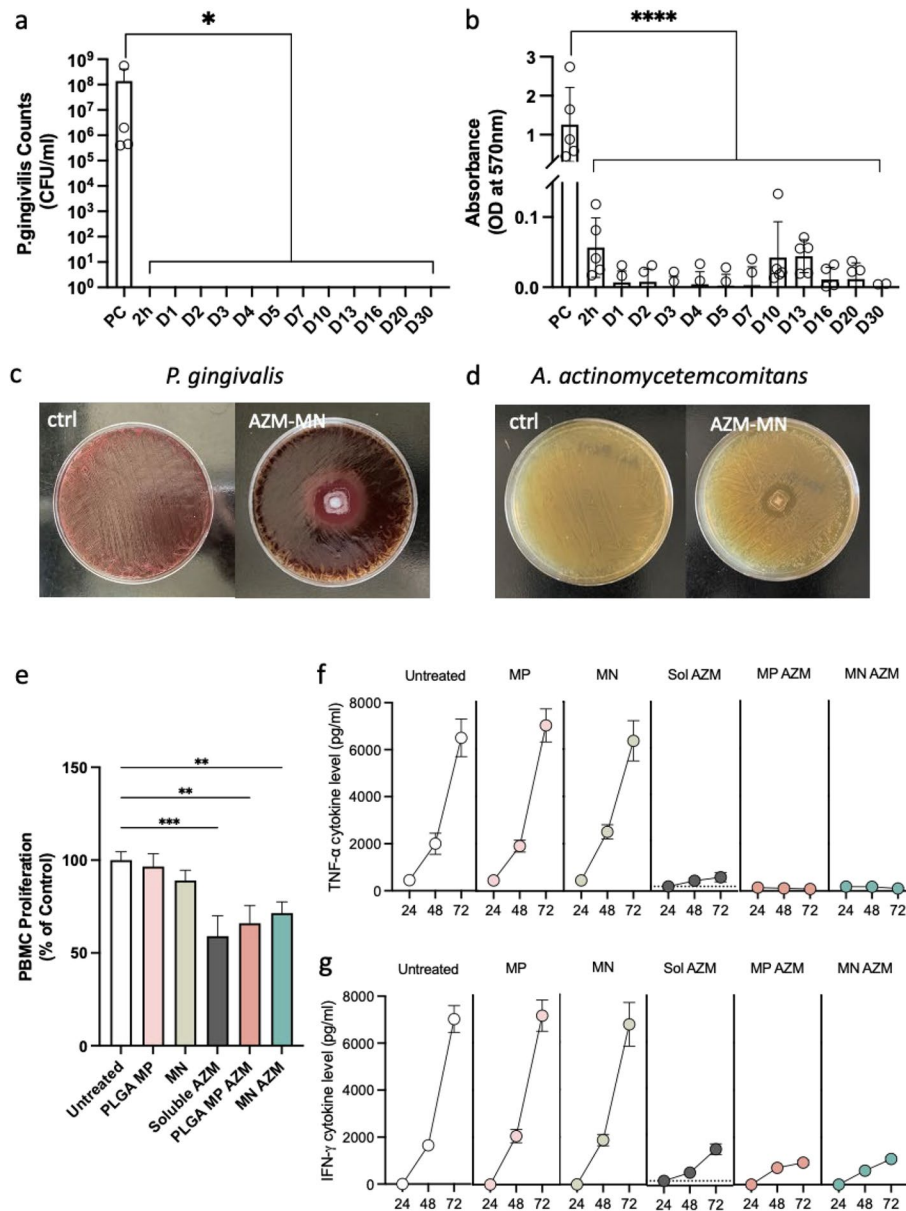


Fig. 3 Sustained release of azithromycin from microneedles *in vitro* shows antibiotic and immunomodulatory effects. **a, b** Supernatants collected from MN release for 30 days were tested against *P. gingivalis*. Bacterial growth and viability were measured by colony-forming unit (CFU) (in a) and 3-(4,5-dimethylthiazol-2-yl)-2,5-diphenyltetrazolium bromide (MTT) assay with absorbance at 570 nm (in b). **c, d** Kirby diffusion assay of MN loaded with AZM MP on bacteria *P. gingivalis* and *A.a.* **e** Proliferation of human PBMCs treated with various formulations was measured. PMSCs were stimulated with ConA and LPS for 3 days. Data are shown as normalized values (percentage of untreated PBMC group). **f, g** Expression of inflammatory cytokines TNF- α and IFN- γ as measured by ELISA. All data are presented as mean \pm SD ($n=4$). Statistical significance is indicated by * $p < 0.05$, ** $p < 0.01$ and *** $p < 0.001$ for differences between samples with different formulations

lymphocytes, monocytes, dendritic cells and macrophages [39]. PBMCs from healthy human donors were stimulated with ConA (for T cell activation) and LPS (for activation of dendritic cells and macrophages) for 3 days to induce immune-activation similar to periodontal diseases. AZM-loaded patches (MN-AZM) and AZM-loaded MPs (MP-AZM) cause suppression of PBMC proliferation (Fig. 3e)

and a drastic inhibition of pro-inflammatory cytokines production by human immune cells (Fig. 3f, g). Such suppression can also promote an anti-inflammatory response in human immune cells and induce regulatory and pro-healing responses. Suppression of inflammatory cytokines such as TNF- α , IL-1 β , IL-12p70 and IL-8 was also observed in murine primary macrophages (Fig. S6).

In vivo evaluation of MN patches for periodontal treatment

We designed the MN patch to simplify delivery of a single small molecule AZM. At the same time, MN patches loaded with IL-4 MPs and a combination of AZM MPs and IL-4 MPs were included in the in vivo efficacy study to investigate the impact of AZM in combination with the additional benefits brought by IL-4. This study provided a foundation to optimize the formulation for clinical use. The efficacy of the MN patches (AZM MN, IL-4 MN, and AZM+IL-4 MN) was tested in vivo by using a ligature-induced periodontitis model in rats. After periodontal disease induction by *A.a.*-coated ligatures, the MN patches were inserted into the periodontal pocket to assess their impact on immunomodulation and tissue regeneration at the cellular and tissue levels.

To examine the in vivo efficacy of antibacterial properties, we first assessed the presence of bacteria in the harvested tissue at the end of eight weeks by using quantitative polymerase chain reaction (qPCR). As shown in Fig. 4a, AZM and AZM+IL-4 MN patches effectively inhibited bacterial growth whereas IL-4 alone patches suppressed bacterial growth to a lesser extent. In addition, the level of pro-inflammatory cytokines such as IL-1 β , tumor necrosis factor α (TNF- α) and IFN- γ were significantly reduced in all three therapeutic groups compared to control MN patches or animals not receiving any treatment (Fig. 4b, c, d). In addition to demonstrating a decrease in the expression of genes encoding inflammatory functions at the end of treatment, the levels of inflammatory cytokines (IL-1 β and TNF- α) in the saliva were found to be significantly reduced over time for the therapeutic patches, as monitored every two weeks during the treatment period (Fig. 4e, f).

Treatment with therapeutic patches not only decreased the levels of inflammatory cytokines, but also increased the expression of anti-inflammatory cytokines such as IL-10 (Fig. 5a) and the regulatory T cell marker, FOXP3 (Fig. 5b). To further examine the local immune cell populations, the harvested gingival tissues were subjected to antibody-staining which indicated a shift in the macrophage population to the M2 phenotype. The AZM group had an elevated number of CD206⁺ macrophages, while the groups treated with IL-4 alone and AZM&IL-4 combined had a substantially greater amount of CD206⁺ macrophages at the diseased sites (Fig. 5c).

Furthermore, therapeutic MN patches induced expression of genes associated with wound healing, including RUNX2 (Runt-related transcription factor 2), COL1A1 (type I collagen α 1), BMP-2 (bone morphogenetic protein 2), and OCN (osteocalcin) (Fig. 6a, b, c, d), indicating an induction of osteogenic activity and collagen matrix synthesis in local periodontal tissues. Bone regeneration at the defect side was

assessed by microcomputed tomography (microCT) eight weeks post-treatment. Reconstructed images of the various treatment groups were used to determine the level of alveolar bone gain at each defect site (Fig. 6e). While rats treated with patches containing only AZM or IL-4 displayed a significant reduction in the distance between the alveolar bone crest and cemento-enamel junction (CEJ) and an increase of alveolar bone volume compared to animals treated with blank patches, the combination of AZM and IL-4 further enhanced the recovery of alveolar bone (Fig. 6f, g). These results supported the effectiveness of AZM and/or IL-4 in reversing bone degeneration in periodontal diseases.

Discussion

Periodontitis is a chronic, destructive and inflammatory disease affecting the tooth-supporting tissues. The ultimate goal of periodontal therapy is to reverse tissue degeneration and regenerate the periodontium. Although pathogenic bacteria are the source of inflammation, recruitment and ineffective reaction of immune cells are the fundamental cause of irresolvable, chronic inflammation. Conventional antibiotics such as the class of tetracycline which are often employed in clinical treatment of periodontitis do not have immune modulatory properties, but our finding shed light on the potential of AZM as a bifunctional therapeutic option due to its dual action of suppressing bacterial growth and modulating immune cells to suppress inflammation. We have successfully engineered a microneedle delivery system comprised of a fast-dissolving patch loaded with biodegradable MPs, which allows for painless and suture-free local placement of the therapeutics. Our results show that the AZM-loaded MN patch alone achieves very positive therapeutic outcomes for periodontal diseases, and the addition of IL-4 MPs can further enhance its efficacy. These results highlight the potential of AZM as a comprehensive treatment option that not only targets the underlying cause of the disease but also supports the regeneration of damaged tissues. Other research studies have also shown the immunomodulatory effects of AZM on macrophage polarization and tissue repair [21, 40, 41]. Interestingly, AZM is naturally accumulated by human cells and was shown to kill intracellular *P. gingivalis* [42]. Using AZM as a starting point, this study provides a promising platform for the treatment of inflammatory disorders, such as periodontitis, and highlights the potential of combining drug delivery systems to improve therapeutic outcomes.

Small molecule immune modulators have the potential to be used in combination with antibiotics. Notably, even without the addition of growth factors, small molecule immune modulators alone can still achieve regenerative effects. While AZM serves as an example of a dual-function agent,

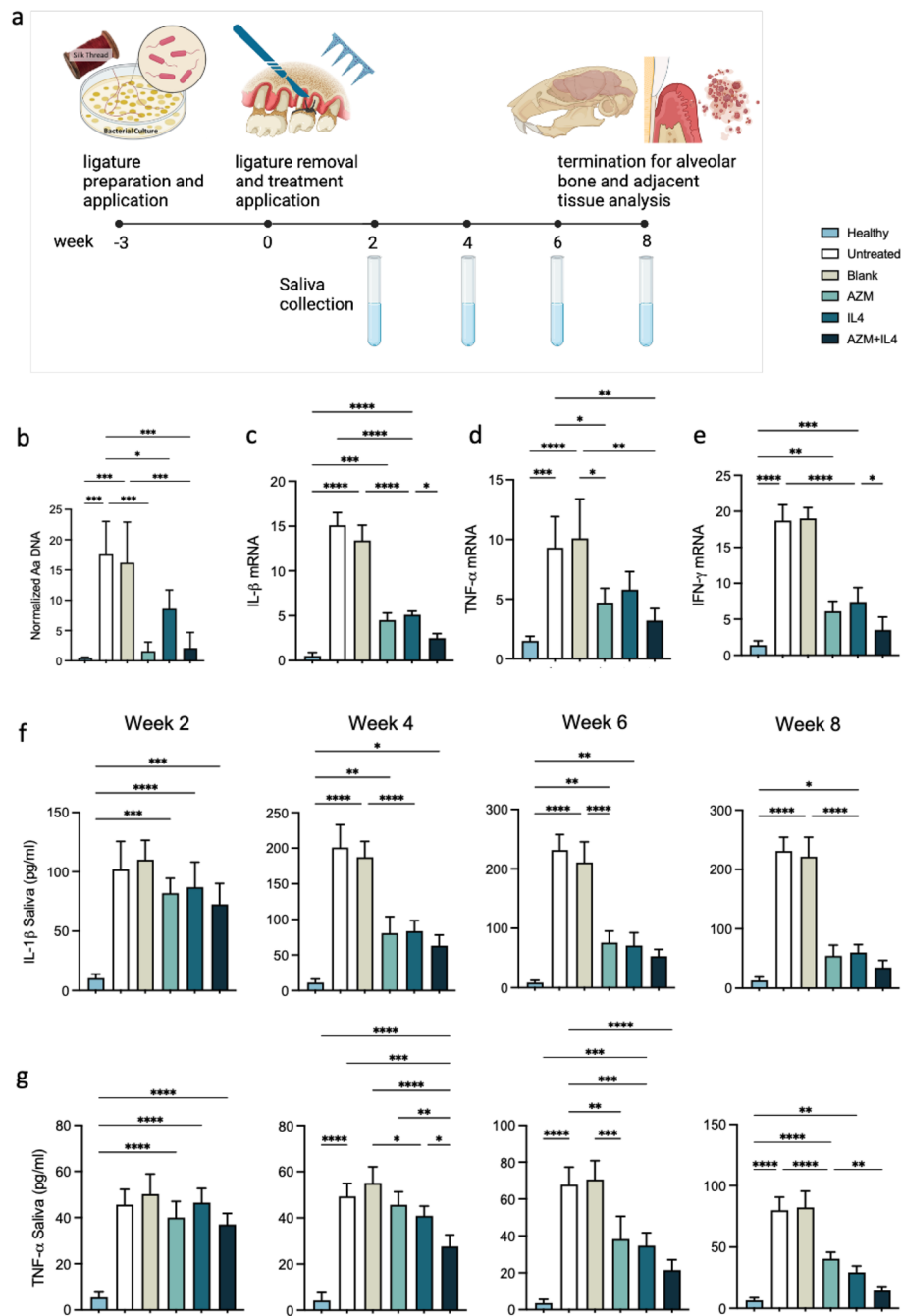


Fig. 4 In vivo evaluation of bacterial growth and inflammation in a rat model of periodontitis. A ligature-induced periodontal disease model in rats was used. **a** schematic timeline of the disease induction, treatments and sample harvests. Briefly, ligatures were inoculated with A.a. and tied to the second molar for three weeks. Ligatures were removed and MN hes were placed at the nearby gingiva by incision. Saliva was collected every two weeks and at eight weeks, surrounding gingival tissues and alveolar bones were harvested for further analysis. **b** PCR analysis of the A.a. bacterial 16S ribosomal DNA in the periodontal tissue normalized by palatal tissue weight. **c-e** mRNA expression of pro-inflammatory cytokine IL-1 β , TNF- α and IFN- γ in periodontal tissues was analyzed by quantitative PCR. mRNA expression levels were normalized to β -actin by the $2^{-\Delta\Delta C_t}$ method. **f** IL-1 β protein level in the saliva was measured by ELISA analysis every two weeks over eight weeks. **g** TNF- α protein level in the saliva was measured by ELISA every two weeks over eight weeks. Healthy, healthy rats; untreated, untreated periodontitis; blank, MN patches without any therapeutic cargo; AZM, MN patches containing azithromycin PLGA MPs (azithromycin, 1 mg; per patch); AZM+IL-4, MN patches containing IL-4 PLGA MPs (IL-4, 40 ng; per patch); AZM+IL-4, MN patches containing both azithromycin and IL-4 PLGA MPs (azithromycin, 1 mg; IL-4, 40 ng; per patch). Data are expressed as mean \pm SD ($n=5$). Results were analyzed by using one-way ANOVA with post hoc analysis. Statistical significance is indicated by asterisks: * $p < 0.05$, ** $p < 0.01$, *** $p < 0.001$ and **** $p < 0.0001$

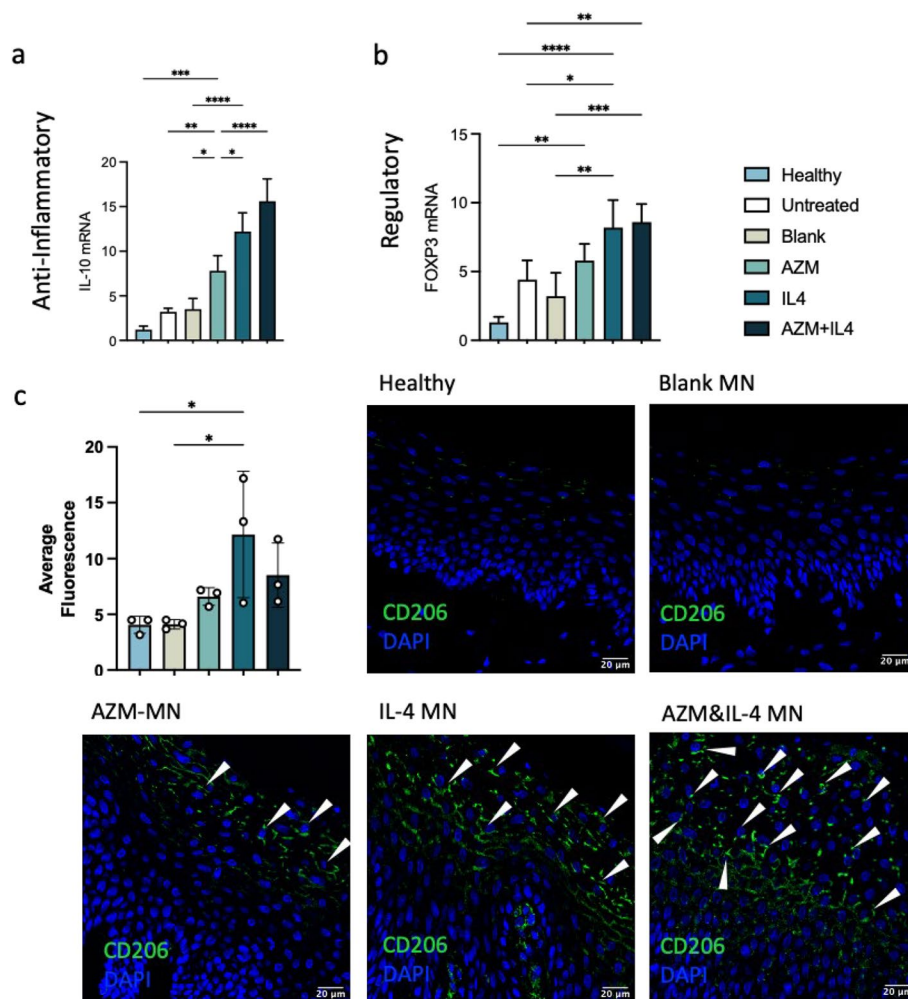


Fig. 5 In vivo evaluation of anti-inflammatory markers and macrophage polarization status. A ligature-induced periodontal disease model in rats was used. **a** Relative mRNA expression level of anti-inflammatory cytokine IL-10. **b** Relative mRNA expression of Treg marker FOXP3. **c** Immunostaining of CD206+ macrophages from harvested tissue. Data were quantified using Fiji and expressed as mean \pm SD ($n=5$). Scale bar represents 20 μ m. Results were analyzed by using one-way ANOVA with post hoc analysis. Statistical significance is indicated by asterisks: * $p < 0.05$, ** $p < 0.01$, *** $p < 0.001$ and **** $p < 0.0001$. White arrows indicate examples of CD206+ cells

the inclusion of more potent small molecule immune modulators alongside antibiotics in a patch can enhance therapeutic efficacy in a combinational manner. By integrating these therapeutic components into a single treatment platform, clinicians can potentially achieve enhanced clinical outcomes, including reduced inflammation, tissue regeneration, and ultimately, improved patient outcomes. On the other hand, by having two different molecular entities for antimicrobial and immunomodulatory effects allows their separation for timed treatment. At the early stage of periodontitis, managing inflammation is beneficial but giving antibiotics may not be desired yet as prescribing an antibiotic introduces the patient to the risk of antibiotic resistance. So, there can be cases where a single immune modulator formulation is preferred to fit the disease progression.

Small molecules, unlike large biologics, are easy to fabricate and store. However, small molecules diffuse quickly and if taken orally, they affect the whole immune system throughout the body. Immune suppression of the whole immune system can put patients into a high-risk state for infection. So, local immune modulation with controlled and prolonged release of immune modulators are desirable, especially for the treatment of localized diseases such as periodontitis. The use of PLGA biodegradable MPs loaded into the microneedle system ensures controlled and sustained release of the antibiotic at the target site for a localized treatment of diseased gingival tissues.

Microarray patches, as a local delivery platform, have been used in various applications including transdermal delivery, ocular delivery, and combinational delivery.

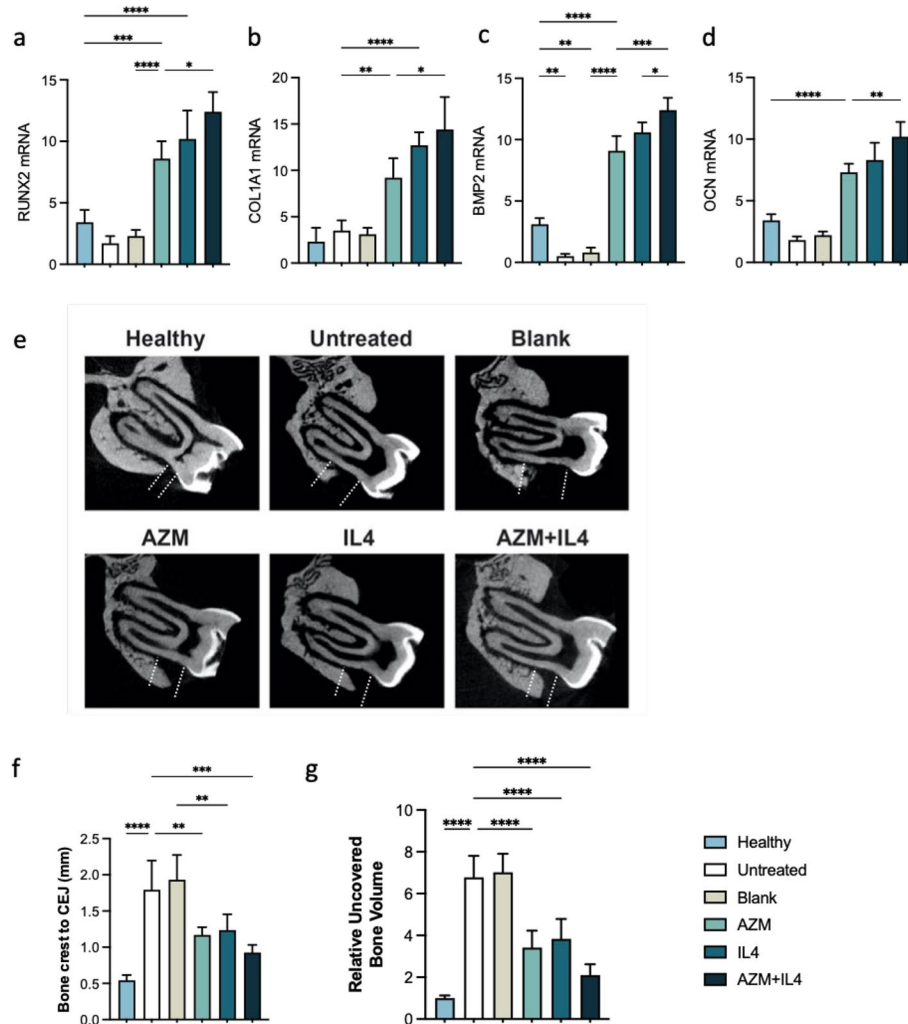


Fig. 6 In vivo evaluation of tissue healing and bone regeneration. In the ligature-induced periodontal disease model in rats, (**a-d**) relative mRNA expression level pro-healing genes RUNX2, COL1A1, BMP-2, and OCN in the periodontal tissue. **e** microCT images of the rat maxilla at 8 weeks after MN implantation. All specimens were normalized, and microCT images were calibrated to enable quantitative comparisons. Dotted line indicates the distance between bone crest and CEJ. **f** Quantitative analysis of vertical bone recovery as determined by measuring the distance between the bone crest and CEJ after 8 weeks of treatment. **g** Relative volumetric bone recovery was calculated by using 3D reconstructed volume at 8 weeks after MN implantation. All data are expressed as mean \pm SD ($n=5$). Results were analyzed by using one-way ANOVA with post hoc analysis. Statistical significance is indicated by asterisks: * $p < 0.05$, ** $p < 0.01$, *** $p < 0.001$ and **** $p < 0.0001$

Inside the oral cavity, it has been used for tongue, gingival and buccal tissues [43]. Unlike local injection, microarray patches have multiple release points rather than a single bolus delivery. It helps with spread of therapeutic loads over a wider range of the diseased area. This novel delivery method enhances the efficiency and effectiveness of treatment while minimizing discomfort for patients. Moreover, by inserting microneedles into the gingival tissue instead of delivery to the dental pocket, we enhance the immunomodulatory effects to host cells and mitigate the risk of bacterial resistance, because bacteria mostly grow in the gingival crevice.

In conclusion, this study contributes to our understanding of periodontitis and proposes a novel treatment approach utilizing AZM as a bifunctional antibiotic/immunomodulatory agent. The use of a microneedle delivery system enhances the targeted and painless administration of the therapeutic agent to the gingival tissue. The dual action of AZM in suppressing bacterial growth and modulating immune responses demonstrates its potential as a comprehensive therapeutic strategy for periodontitis. These findings provide a basis for further research and potentially pave the way for the development of novel and effective treatment options for this prevalent oral disease and more chronic inflammatory diseases.

Materials and methods

Chemicals and biologicals

All chemicals were purchased from Sigma-Aldrich unless noted otherwise. Glassware was acid-cleaned overnight and then thoroughly rinsed with Milli-Q water. Cell culture reagents, solutions, and dishes were obtained from Thermo Fisher Scientific unless specified otherwise.

PLGA microparticle synthesis

Acid terminated PLGA (200 mg; 50:50 lactic acid-to-glycolic acid ratio) was dissolved and stirred in 5 ml dichloromethane (DCM) overnight. To fabricate AZM MPs via a single emulsion method, 15 mg AZM was added to 5 ml PLGA-DCM mixture. A 10-fold volume of 1% polyvinyl alcohol (PVA) was added right before homogenization at 5000 rpm for 10 min. To fabricate IL-4 MPs via a double emulsion method, primary emulsion (water-in-oil) was formed by adding 10 μg (200 μl of 50 $\mu\text{g}/\text{ml}$) IL-4 aqueous solution to 4 ml of 40 mg/ml PLGA organic solvents and the mixture was sonicated using Q500 Sonicator (Qsonica, Newtown, CT) with 1/2" Probe at 40% power for 2 min with a cycle of 4-s on and 2-s off. Next, secondary emulsion (oil-in-water) was formed by slowly adding 1% PVA to the primary emulsion. The secondary emulsion was homogenized at 5000 rpm for 10 min.

For both AZM and IL-4 MP, the homogenized solutions were poured into tenfold volume of 0.1% PVA and stirred for 4 h in open air to evaporate the organic solvents. Low-speed centrifugation (2000 rpm, 5 min) was performed three times to wash and remove undesired clumps. Precipitated MPs were preserved at 4 °C for short-term use and at -20 °C for long-term use. *In vitro* release of AZM and IL-4 were studied by incubating 10 mg of either AZM or IL-4 loaded PLGA microparticles in 1 mL of PBS (pH 7.4) at 37 °C under gentle stirring. At different time intervals, stirring was stopped and 1 μL of the supernatant was taken from the sample. The concentration of released AZM was determined by measuring the absorbance at 553 nm wavelength using UV-vis spectrophotometer (Thermo Scientific NanoDrop One). IL-4 concentration was measured using LEGEND Max Mouse IL-4 ELISA Kit (BioLegend) following manufacturer's instruction.

MN patch fabrication

MN molds were purchased from Micropoint Technologies (Singapore) with 11 \times 11 microneedle array in pyramid shape needle of 200 μm base diameter, 750 μm height and 500 μm tip-to-tip spacing. The MN fabrication process is illustrated

in Fig. S7. To fabricate MN patches, 70% ethanol was cast on negative PDMS molds and subjected to vacuum for 5 min. Following the removal of bubbles and excess ethanol, 100 μl suspension of MPs (1 mg) in 20% PVP and 0.75% glycerol were cast into the well of the mold. MN patches were air dried at room temperature overnight. The time needed for this process can be reduced by air-drying the MN patches for 6 h followed by further drying under vacuum for 2 h. Solidified MN patches were peeled off from the molds and stored at 4 °C until use or -20 °C when IL-4 were present.

Mechanical property of MNs

The mechanical strength of MNs was measured by a compression test on a low-force mechanical testing system (5943 MicroTester, Instron). The MN tips were placed perpendicularly to the stainless-steel plate and were pressed against another stainless-steel plate moving at a constant speed of 0.5 mm/minute. Correlations between the applied force and the deformation of the MNs were recorded. All tests were performed in triplicate.

Kirby-Bauer agar disk diffusion assay

The Kirby-Bauer agar disk diffusion assay was used to test the antibacterial properties of drugs against *P. gingivalis* and *A.a.* (D7SS strain). Discs containing known amounts of compounds were prepared by adding calculated amount of the corresponding solution (*i.e.* PBS, azithromycin, tofacitinib, lupeol and dexamethasone) to 8 mm sterile paper disks. These paper disks were air-dried in a biosafety cabinet before use. Further, the disks and MN patches were placed on agar plates onto which 10^7 bacterial cells were already spread. Columbia Broth with Hemin and menadione was used for liquid culture overnight growth of *P. gingivalis* and Tryptic Soy Broth with yeast extract (TSBY) was used for *A.a.*. The bacterial plates were incubated under anaerobic conditions (10% CO_2 , 10% H_2 , and 80% N_2) at 37 °C and the inhibition zones were measured after 1 and 5 days for *A.a.* and after 7 and 20 days for *P. gingivalis*.

Liquid antibacterial assay

Supernatants were collected from AZM MN patches immersed in 1 ml of PBS for varying length of time up to 30 days. To set up the assay, 500 μl of the supernatants was combined with 500 μl of 2 \times concentrated bacterial culture medium containing a final concentration of 5×10^7 bacterial cells per well in a 48-well culture plate. After three days of growing under anaerobic conditions (10% CO_2 , 10% H_2 , and 80% N_2) at 37 °C, an aliquot of 100 μl was removed from each of these wells for further analysis.

For Colony-forming Unit (CFU) analysis, the 100 μ l aliquot (bacterial culture grown in the presence of the various supernatants for 3 days) was serially diluted six times in ten-fold steps. From each of the dilutions, 100 μ l was plated onto the appropriate agar plates. The plates were incubated under anaerobic conditions (10% CO₂, 10% H₂, and 80% N₂) for 2 and 5 days for *A.a.* and *P. gingivalis* respectively. After this incubation period, all colonies were counted and analyzed.

The viability of bacterial cells treated with supernatants from AZM MN patches was analyzed with the MTT assay. Briefly, 5 mg/ml MTT [3-(4,5-dimethylthiazol-2-yl)-2,5-diphenyl tetrazolium bromide, Sigma-Aldrich, St. Louis, MO] solution was aseptically prepared by dissolving the MTT powder in sterile PBS at room temperature and stored at 4 °C in a dark, screw-cap container. Simultaneously with the CFU analysis, an aliquot of 100 μ l from each of the suspensions was placed into a 96-well plate and 10 μ l of MTT solution was added to each well. The 96-well plate was then incubated for 2 h at 37 °C at 120 rpm in a shaker in the dark. After the incubation period, an equal amount of dimethyl sulfoxide (100 μ l) was added to each well to solubilize formazan the insoluble purple cleavage product of MTT generated through the metabolism of live cells. The levels of microbial metabolic activity in the suspensions were determined by measuring the absorbance at OD₅₇₀ nm.

Isolation of bone marrow-derived macrophages

All cell isolation experiments on mice and rats were performed under a protocol approved by the Institutional Animal Care and Use Committee (IACUC) at the University of California, Los Angeles (UCLA) and in accordance with UCLA's institutional policy on the humane and ethical treatment of animals. Eight- to ten-week-old wild-type (C57BL/6) mice were purchased from The Jackson Laboratory and eight- to ten-week-old wildtype (Sprague Dawley) rats were purchased from Charles River Laboratories. Animals were maintained in specific pathogen-free facilities at UCLA.

Ten-week-old C57BL/6 mice or Sprague Dawley rats were euthanized, and hindlimbs were harvested in PBS. Under sterile conditions, muscles were scraped off, and the ends of the bones were cut off. Bone marrow was flushed into a sterile 50 ml conical tube with 2 ml Dulbecco's modified Eagle's medium (DMEM)/F12 supplemented with 10% fetal bovine serum and 1% penicillin–streptomycin. Cells were pelleted and plated with 50 ng/ml mouse/rat macrophage colony stimulating factor (BioLegend). Following 3 days of incubation, 5 ml fresh complete DMEM/F12 medium with 25 ng/ml macrophage colony stimulating factor was supplied per 10 cm cell culture dish. Cells were again incubated for 3 more days. Then supernatants were discarded, and dishes were washed with PBS three times to

remove non-adherent cells. BMDMs were gently scraped off the dish, pelleted, counted, and seeded in new plates for further macrophage polarization and experimentation. LPS (10 ng/ml was used to induce pro-inflammatory (M1) macrophages, while 25 ng/ml IL-4 was used to induce pro-healing (M2) macrophages. Complete DMEM/F12 medium alone served as control.

In vitro proliferation and activation of human PBMCs

2×10^5 PBMCs/well were plated in 96-well flat-bottom tissue-culture plates. Cells were incubated for a total of 3 days after 4 h of stimulation with concanavalin A (ConA 1 μ g/ml; Millipore Sigma), lipopolysaccharide (LPS from *Escherichia coli* O111:B4, 1 μ g/ml; Millipore Sigma) in complete RPMI medium at 37 °C in a 5% CO₂ atmosphere. Lymphocyte proliferation was measured using 5-bromo-2'-deoxyuridine (BrdU) Cell Proliferation ELISA colorimetric Kit (Abcam). The culture supernatants were collected for the analysis of cytokine secretion using ELISA per manufacturer's instruction.

RNA isolation, reverse transcription and qPCR

Total RNA was extracted by using TRIzol reagent (Life Technologies, Gaithersburg, MD, U.S.A.), and the concentration was determined by spectrophotometric optical density measurement (Thermo Scientific NanoDrop). The OD₂₆₀/OD₂₈₀ ratio in all samples ranged between 1.7 and 2.0 to ensure RNA purity. Reverse transcription was then carried out using Maxima SYBR Green qPCR master mix according to manufacturer's suggested protocol. The cDNA was stored at –20 °C. PCR was performed by using SYBR Green kit according to manufacturer's suggested protocol on BioRad CFX96 PCR detection system. Primer sequences were as following:

GAPDH- Forward 5' CATCACTGCCACCCAGAA
GACTG Reverse 5' ATGCCAGTGAGCTTCCCCGTTTCAG;

iNOS – Forward 5' GAGACAGGGAAGTCTGAAGCAC
Reverse 5' CCAGCAGTAGTTGCTCCTCTTC.

Animal study

All tissue regeneration experiments on mice and rats were performed under protocols approved by the IACUC at UCLA or University of Alabama at Birmingham (UAB) and in accordance with the institutional policy of UCLA and UAB on the humane and ethical treatment of animals throughout the study design, implementation, and data analysis phases. Eight- to ten-week-old Sprague Dawley rats were purchased from Charles River Laboratories.

In vivo functionality of the designed MNs was evaluated using a rat periodontal defect model, as described previously with some modifications [44, 45]. Virgin male and female Sprague Dawley rats (Harlan Laboratories, Livermore, CA) were utilized for in vivo testing of the proposed periodontal treatments according to approved animal protocols. The animals were divided into six groups (five rats per group): (i) healthy control, (ii) no treatment (untreated), (iii) blank MN, (iv) AZM MN containing azithromycin, (v) IL-4 MN containing interleukin-4, and (vi) AZM + IL-4 MN, containing azithromycin and IL-4. We did not include an experimental group with a direct injection of MPs containing AZM because such an injection might require a large volume, which is not feasible for gum tissue, and the injected MPs might not be retained in the local tissues, making comparison with other groups challenging. The number of animals in each experimental group was determined based on a power analysis to ascertain the minimal number of rats needed to detect significant changes, such as bacteria inhibition and anti-inflammatory cytokine induction by MNs containing AZM.

Briefly, mucoperiosteal flaps were elevated in rats in groups (ii-vi), uncovering the alveolar bone adjacent to the mesiolingual aspect of the first maxillary molars. The alveolar bone covering the root surfaces on the lingual side was removed with a dental bur under constant saline irrigation, and an *A.a.*-coated 5–0 silk ligature was tied around the left second molar. The silk ligature was inoculated with *A.a.* under anaerobic conditions for 24 h before the procedure. Three weeks later, designed patches were inserted into the defect site as noted above for groups. Eight weeks post-implantation, the animals were sacrificed and the amounts of bone regeneration at defect sites were evaluated using μ CT analysis. All the specimens were standardized, and μ CT images were calibrated for proper comparative analysis. The vertical bone loss at each defect site was evaluated by measuring the distance between the cemento-enamel junction (CEJ) and alveolar bone crest as well as the relative alveolar bone area according to methods reported in the literature [46].

Characterization of inflammatory responses at the defect sites

At different time intervals after implantation, five sterile paper points (Patterson Dental) were placed around the patch insertion sites to collect saliva (under general anesthesia) for at least 30 s, and the concentrations of inflammatory cytokines and anti-inflammatory cytokines were measured using enzyme-linked immunosorbent assay (ELISA) kits.

For endpoint analysis, the expression of cytokines at the defect sites were analyzed by collecting the periodontal

tissue as described previously [44]. Briefly, at 8 weeks post-implantation, buccal and palatal tissues of maxillary molars were isolated and dissociated using collagenase and DNase I (50 μ g/ml) at 37 °C for 15 min. These enzymes were then inactivated with EDTA (20 μ l/ml of solution). Tissues were then disaggregated and passed through a 100- μ m cell strainer to obtain a single-cell suspension. Quantitative PCR assays were used to analyze gene expression. RNA from isolated cells was isolated using Trizol reagent. RNA was reverse-transcribed and single-stranded cDNA was made using a Superscript III cDNA synthesis kit. Relative gene expression was calculated using the $2^{-\Delta\Delta C_t}$ method, with normalization to the *Ct* of the housekeeping gene beta actin. Quantification of *A.a.* in the periodontal tissues was performed as previously reported [44]. The concentrations of inflammatory and anti-inflammatory cytokines were measured by using ELISA kits after the extraction of proteins from the gingival tissue by tissue homogenization.

Statistical analysis

The one-way ANOVA and two-tailed Student's t-test were utilized as appropriate to analyze the data at a significance of α or $p < 0.05$. Quantitative data are expressed as mean \pm SD. To determine the number of specimens for the proposed experiments, power analysis was conducted based on our preliminary data.

Supplementary Information The online version contains supplementary material available at <https://doi.org/10.1007/s44258-024-00023-5>.

Acknowledgements The authors would like to acknowledge the University of California, Los Angeles and the Troy University. Fig. 4a were generated using Biorender.com.

Authors' contributions X.Z., M.M.H.-S., and S.L. conceived the presented idea and designed experiments. X.Z. performed experiments, analyzed the data and wrote the paper. M.M.H.-S., R.F., and I.H. contributed to some *in vitro* experiments. B.S. and R.L. contributed to bacteria experiments. E.D., F.F., O.B., and T.A. contributed to animal experiments. All authors edited the manuscript.

Funding This work is supported in part by grants from the National Institute of Dental & Craniofacial Research (R56DE029157), Center for Dental, Oral and Craniofacial Tissue Organ Regeneration (U24 DE026914), Eli and Edythe Broad Center of Regenerative Medicine and Stem Cell Research Award Program, and National Institute of Diabetes and Digestive and Kidney Diseases (R01DK112939). The contents of this publication are solely the responsibility of the authors and do not necessarily represent the official views of NIH, or/and other agency of the State of California.

Availability of data and materials Lead contact: Song Li (songli@ucla.edu).

Materials availability: This study did not generate new unique materials.

Data and code availability: All data associated with this study are present in the paper or the Supplemental Information. Raw data are available upon request.

Declarations

Ethics approval and consent to participate Not applicable.

Consent for publication All authors have read and agreed to the published version of the manuscript.

Competing interests The Regents of the University of California filed patent applications (periodontal micropatch and uses thereof, U.S. Provisional Patent Application PCT/US20/58069) related to this study, with X.Z., M.M.H.-S. and S.L. as inventors. X.Z., M.M.H.-S. and S.L. are founders and equity holders in Locagen Therapeutics. S.L. is the Editor-in-chief for Med-X. The paper was handled by the other Editor and has undergone a rigorous peer review process. The other authors declare no potential conflicts of interest with respect to the authorship and/or publication of this article.

Open Access This article is licensed under a Creative Commons Attribution 4.0 International License, which permits use, sharing, adaptation, distribution and reproduction in any medium or format, as long as you give appropriate credit to the original author(s) and the source, provide a link to the Creative Commons licence, and indicate if changes were made. The images or other third party material in this article are included in the article's Creative Commons licence, unless indicated otherwise in a credit line to the material. If material is not included in the article's Creative Commons licence and your intended use is not permitted by statutory regulation or exceeds the permitted use, you will need to obtain permission directly from the copyright holder. To view a copy of this licence, visit <http://creativecommons.org/licenses/by/4.0/>.

References

- Kinane DF, Stathopoulou PG, Papapanou PN. Periodontal diseases. *Nat Rev Dis Prim*. 2017;3:17038. <https://doi.org/10.1038/nrdp.2017.38>.
- Eke PI, Dye BA, Wei L, Thornton-Evans GO, Genco RJ. Prevalence of periodontitis in adults in the United States: 2009 and 2010. *J Dent Res*. 2012;91(10):914–20. <https://doi.org/10.1177/0022034512457373>.
- Hajishengallis G, Darveau RP, Curtis MA. The keystone-pathogen hypothesis. *Nat Rev Microbiol*. 2012;10(10):717–25. <https://doi.org/10.1038/nrmicro2873>.
- Hajishengallis G, Lamont RJ. Beyond the red complex and into more complexity: the polymicrobial synergy and dysbiosis (PSD) model of periodontal disease etiology. *Mol Oral Microbiol*. 2012;27(6):409–19. <https://doi.org/10.1111/j.2041-1014.2012.00663.x>.
- Yang B, Pang X, Li Z, Chen Z, Wang Y. Immunomodulation in the Treatment of Periodontitis: Progress and Perspectives. *Front Immunol*. 2021;12:781378. <https://doi.org/10.3389/fimmu.2021.781378>.
- Xu W, Zhou W, Wang H, Liang S. Roles of *Porphyromonas gingivalis* and its virulence factors in periodontitis. *Adv Protein Chem Struct Biol*. 2020;120:45–84. <https://doi.org/10.1016/bs.apcsb.2019.12.001>.
- Li N, Collyer CA. Gingipains from *Porphyromonas gingivalis* - Complex domain structures confer diverse functions. *Eur J Microbiol Immunol (Bp)*. 2011;1(1):41–58. <https://doi.org/10.1556/EuJMI.1.2011.1.7>.
- J. S. Marschall, "Porphyromonas gingivalis gingipains induce a pro-inflammatory extracellular microenvironment : the role of PAR-2 and fibronectin.," 2016.
- Sun X, Gao J, Meng X, Lu X, Zhang L, Chen R. Polarized Macrophages in Periodontitis: Characteristics, Function, and Molecular Signaling. *Front Immunol*. 2021;12:763334. <https://doi.org/10.3389/fimmu.2021.763334>.
- Jiang Q, et al. Interactions Between Neutrophils and Periodontal Pathogens in Late-Onset Periodontitis. *Front Cell Infect Microbiol*. 2021;11:627328. <https://doi.org/10.3389/fcimb.2021.627328>.
- Scott DA, Krauss J. Neutrophils in periodontal inflammation. *Front Oral Biol*. 2012;15:56–83. <https://doi.org/10.1159/000329672>.
- Feng Y, et al. Role of Interleukin-17A in the Pathomechanisms of Periodontitis and Related Systemic Chronic Inflammatory Diseases. *Front Immunol*. 2022;13:862415. <https://doi.org/10.3389/fimmu.2022.862415>.
- González-Osuna L, et al. Senescent CD4(+)CD28(-) T Lymphocytes as a Potential Driver of Th17/Treg Imbalance and Alveolar Bone Resorption during Periodontitis. *Int J Mol Sci*. 2022;23(5):2543. <https://doi.org/10.3390/ijms23052543>.
- Yin L, Li X, Hou J. Macrophages in periodontitis: A dynamic shift between tissue destruction and repair. *Jpn Dent Sci Rev*. 2022;58:336–47. <https://doi.org/10.1016/j.jdsr.2022.10.002>.
- Cheng W-C, et al. Periodontitis-associated pathogens *P. gingivalis* and *A. actinomycetemcomitans* activate human CD14(+) monocytes leading to enhanced Th17/IL-17 responses. *Eur J Immunol*. 2016;46(9):2211–21. <https://doi.org/10.1002/eji.201545871>.
- Ilango P, Kumar D, Mahalingam A, Thanigaimalai A, Reddy VK. Evidence revealing the role of T cell regulators (Tregs) in periodontal diseases: A review. *J Indian Soc Periodontol*. 2021;25(4):278–82. https://doi.org/10.4103/jisp.jisp_308_20.
- Li Y, Ling J, Jiang Q. Inflammasomes in Alveolar Bone Loss. *Front Immunol*. 2021;12:691013. <https://doi.org/10.3389/fimmu.2021.691013>.
- Hathaway-Schrader JD, Novince CM. Maintaining homeostatic control of periodontal bone tissue. *Periodontol 2000*. 2021;86(1):157–87. <https://doi.org/10.1111/prd.12368>.
- Zhang X, et al. Immunomodulatory microneedle patch for periodontal tissue regeneration. *Matter*. 2022;5(2):666–82. <https://doi.org/10.1016/j.matt.2021.11.017>.
- Murphy BS, Sundareshan V, Cory TJ, Hayes DJ, Anstead MI, Feola DJ. Azithromycin alters macrophage phenotype. *J Antimicrob Chemother*. 2008;61(3):554–60. <https://doi.org/10.1093/jac/dkn007>.
- Haydar D, et al. Azithromycin Polarizes Macrophages to an M2 Phenotype via Inhibition of the STAT1 and NF-κB Signaling Pathways. *J Immunol*. 2019;203(4):1021–30. <https://doi.org/10.4049/jimmunol.1801228>.
- Wang J, Xie L, Wang S, Lin J, Liang J, Xu J. Azithromycin promotes alternatively activated macrophage phenotype in systemic lupus erythematosus via PI3K/Akt signaling pathway. *Cell Death Dis*. 2018;9(11):1080. <https://doi.org/10.1038/s41419-018-1097-5>.
- Lee JW, Prausnitz MR. Drug delivery using microneedle patches: not just for skin. *Expert Opin Drug Deliv*. 2018;15(6):541–3. <https://doi.org/10.1080/17425247.2018.1471059>.
- Sartawi Z, Blackshields C, Faisal W. Dissolving microneedles: Applications and growing therapeutic potential. *J Control Release*. 2022;348:186–205. <https://doi.org/10.1016/j.jconrel.2022.05.045>.
- Zhu Y, et al. The pentacyclic triterpene Lupeol switches M1 macrophages to M2 and ameliorates experimental inflammatory bowel disease. *Int Immunopharmacol*. 2016;30:74–84. <https://doi.org/10.1016/j.intimp.2015.11.031>.
- Shiratori H, et al. An in vitro test system for compounds that modulate human inflammatory macrophage polarization. *Eur J Pharmacol*. 2018;833:328–38. <https://doi.org/10.1016/j.ejphar.2018.06.017>.

27. Jiang K, Weaver JD, Li Y, Chen X, Liang J, Stabler CL. Local release of dexamethasone from macroporous scaffolds accelerates islet transplant engraftment by promotion of anti-inflammatory M2 macrophages. *Biomaterials*. 2017;114:71–81. <https://doi.org/10.1016/j.biomaterials.2016.11.004>.
28. Hirsch R, Deng H, Laohachai MN. Azithromycin in periodontal treatment: more than an antibiotic. *J Periodontol Res*. 2012;47(2):137–48. <https://doi.org/10.1111/j.1600-0765.2011.01418.x>.
29. Chiu Y-S, et al. The JAK inhibitor Tofacitinib inhibits structural damage in osteoarthritis by modulating JAK1/TNF-alpha/IL-6 signaling through Mir-149-5p. *Bone*. 2021;151:116024. <https://doi.org/10.1016/j.bone.2021.116024>.
30. Saleem M. Lupeol, a novel anti-inflammatory and anti-cancer dietary triterpene. *Cancer Lett*. 2009;285(2):109–15. <https://doi.org/10.1016/j.canlet.2009.04.033>.
31. Gensler LS. Glucocorticoids: complications to anticipate and prevent. *The Neurohospitalist*. 2013;3(2):92–7. <https://doi.org/10.1177/1941874412458678>.
32. Ai F, Zhao G, Lv W, Liu B, Lin J. Dexamethasone induces aberrant macrophage immune function and apoptosis. *Oncol Rep*. 2020;43(2):427–36. <https://doi.org/10.3892/or.2019.7434>.
33. Sinha S, Kumar S, Dagli N, Dagli RJ. Effect of tetracycline HCl in the treatment of chronic periodontitis - A clinical study. *J Int Soc Prev Community Dent*. 2014;4(3):149–53. <https://doi.org/10.4103/2231-0762.142011>.
34. Amarnani R, Shende P. Microneedles in diagnostic, treatment and theranostics: An advancement in minimally-invasive delivery system. *Biomed Microdevices*. 2021;24(1):4. <https://doi.org/10.1007/s10544-021-00604-w>.
35. Mangang KN, et al. PVP-microneedle array for drug delivery: mechanical insight, biodegradation, and recent advances. *J Biomater Sci Polym Ed*. 2023;34(7):986–1017. <https://doi.org/10.1080/09205063.2022.2155778>.
36. Shim WS, Hwang YM, Park SG, Lee CK, Kang NG. Role of Polyvinylpyrrolidone in Dissolving Microneedle for Efficient Transdermal Drug Delivery: In vitro and Clinical Studies. *Bull Korean Chem Soc*. 2018;39(6):789–93. <https://doi.org/10.1002/bkcs.11476>.
37. vander Straeten A, et al. A microneedle vaccine printer for thermostable COVID-19 mRNA vaccines. *Nat Biotechnol*. 2023;42(3):510–7. <https://doi.org/10.1038/s41587-023-01774-z>.
38. Kaplan JB, Rangunath C, Ramasubbu N, Fine DH. Detachment of *Actinobacillus actinomycetemcomitans* biofilm cells by an endogenous beta-hexosaminidase activity. *J Bacteriol*. 2003;185(16):4693–8. <https://doi.org/10.1128/JB.185.16.4693-4698.2003>.
39. Pourahmad J, Salimi A. Isolated Human Peripheral Blood Mononuclear Cell (PBMC), a Cost Effective Tool for Predicting Immunosuppressive Effects of Drugs and Xenobiotics. *Iran J Pharm Res*. 2015;14(4):979.
40. Zhang B, Bailey WM, Kopper TJ, Orr MB, Feola DJ, Gensel JC. Azithromycin drives alternative macrophage activation and improves recovery and tissue sparing in contusion spinal cord injury. *J Neuroinflammation*. 2015;12:218. <https://doi.org/10.1186/s12974-015-0440-3>.
41. Heidary M, et al. Mechanism of action, resistance, synergism, and clinical implications of azithromycin. *J Clin Lab Anal*. 2022;36(6):e24427. <https://doi.org/10.1002/jcla.24427>.
42. Lai P-C, Walters JD. Relative effectiveness of azithromycin in killing intracellular *Porphyromonas gingivalis*. *Clin Exp Dent Res*. 2016;2(1):35–43. <https://doi.org/10.1002/cre2.17>.
43. Lee KJ, et al. Non-transdermal microneedles for advanced drug delivery. *Adv Drug Deliv Rev*. 2020;165–166:41–59. <https://doi.org/10.1016/j.addr.2019.11.010>.
44. Glowacki AJ, et al. Prevention of inflammation-mediated bone loss in murine and canine periodontal disease via recruitment of regulatory lymphocytes. *Proc Natl Acad Sci*. 2013;110(46):18525–30. <https://doi.org/10.1073/pnas.1302829110>.
45. Hasani-Sadrabadi MM, et al. Hierarchically Patterned Polydopamine-Containing Membranes for Periodontal Tissue Engineering. *ACS Nano*. 2019;13(4):3830–8. <https://doi.org/10.1021/acsnano.8b09623>.
46. Hasani-Sadrabadi MM, et al. An engineered cell-laden adhesive hydrogel promotes craniofacial bone tissue regeneration in rats. *Sci Transl Med*. 2020;12(534):eaay6853. <https://doi.org/10.1126/scitranslmed.aay6853>.

Publisher's Note Springer Nature remains neutral with regard to jurisdictional claims in published maps and institutional affiliations.